Second-generation photocatalytic materials: anion-doped TiO$_2$

Second-generation photocatalytic materials: anion-doped TiO$_2$

H Wang and J P Lewis

Department of Physics and Astronomy, Brigham Young University, Provo, UT 84602, USA

Abstract
Previous experimental studies describe an efficient photoresponse in the visible-light region for anion-doped TiO$_2$. Doping with carbon, nitrogen, as well as sulfur, yields promising second-generation photocatalysis with TiO$_2$. We present a theoretical investigation of substitutional anion doping in TiO$_2$ and discuss doping effects on the electronic structure, and subsequently the photoactivity. The resulting bandgap narrowing predicted in this work is consistent with experimental observations. Furthermore, we discuss the effects of doping concentration on the localization properties of the valence band edge. Our systematic study of anion-doped TiO$_2$ implies that the carbon-doped TiO$_2$ is the most promising due to a significant overlap between the O 2p state and the carbon states near the valence band edge. Additionally, carbon dopants produce the largest valence band red shift of the three anion-doped TiO$_2$ studied.

1. Introduction

The evidence of photoelectrochemical splitting of water over TiO$_2$ to form H$_2$ and O$_2$ by Fujishima and Honda [1] in 1972 opened up greater possibilities of solar energy conversion of materials by semiconductors. The other environmental applications, such as self-cleaning of tiles, glass, and windows, air purification, deodorization, and sterilization, have also attracted extensive interest [2–10]. TiO$_2$ has several advantages due to its high chemical stability, excellent functionality, nontoxicity, and relatively low price, but a serious disadvantage is that only UV light can be used for its photocatalytic capabilities. Only about 3% of the solar spectrum can be utilized due to its wide intrinsic band gap. Therefore, it is of great interest to find ways to extend the absorption wavelength range of TiO$_2$ into the visible region without decrease of photocatalytic activity.

Many techniques have been examined to extend the spectral response of TiO$_2$ into the visible region and enhance its photocatalytic activity. Impurity doping is one of the typical approaches to extend the spectral response of a wide band gap semiconductor to visible light. Various transition-metal cation dopants have been extensively studied (for example, see [11–14]). Except for a few cases [12, 13], the photocatalytic activities of a cation-doped

TiO$_2$ decreased even in the UV region. This is because the doped TiO$_2$ suffers from a thermal instability or an increase in the recombination centres of the charge carriers introduced by the dopants' localized d-states deep in the band gap of TiO$_2$ [11].

Thus, anionic nonmetal dopants, such as carbon [15–19], nitrogen [20–25], and sulfur [26–29], may be more appropriate for the extension of photocatalytic activity into the visible-light region because the related impurity states are near the valence band edge, but do not act as charge carriers. Furthermore, their role as recombination centres might be minimized as compared to cation doping. Results for doping with both C and N indicate about a 50 nm red shift in the absorption spectra [15–18, 20], and the production of photoactivity in the visible. Recent results with carbon further demonstrate improved photocatalysis efficiency in water splitting [16].

The optical and photocatalytic properties of those anion-doped TiO$_2$ have been studied in detail [15–18, 27], but their fundamental mechanisms have still not been well understood. Light absorption is largely a factor of the electronic structures of materials. The experimental results [15–18, 20–23, 26, 27] also imply that anionic nonmetal dopants can provide an effective modification to the electronic structure of TiO$_2$. In this work, we explore the electronic properties of anion (C, N, and S)-doped TiO$_2$ materials using an *ab initio* tight-binding method, called FIREBALL, which is based on density-functional theory (DFT) with a nonlocal pseudopotential scheme [30]. This method has been successfully applied to a number of systems, such as zeolites, clathrate structures, semiconducting materials, and biomolecules [30–34]. Our calculations provide an initial glance into the electronic properties required for acceptable photocatalysis.

2. Computational method

FIREBALL is a first-principles tight-binding molecular dynamics (TBMD) simulation technique based on a self-consistent version of the Harris–Foulkes [35, 36] functional [32]. In this method, confined atomic-like orbitals are used as a basis set for the determination of the occupied eigenvalues and eigenvectors of the one-electron Hamiltonian. The 'fireball' orbitals, introduced by Sankey and Niklewski [37], are obtained by solving the atomic problem with the boundary condition that the atomic orbitals vanish outside and at a predetermined radius r_c where wavefunctions are set to be zero. This boundary condition is equivalent to an 'atom in the box' and has the effect of raising the electronic energy levels due to confinement. An important advantage of the Sankey and Niklewski basis set is that the Hamiltonian and the overlap matrix elements of the system are quite sparse for large systems, reducing the overall computation time. On the other hand, the light excitation of the atoms somewhat accounts for Fermi compression in a solid which apparently gives a better representation of solid-state charge densities [38]. For this work, we chose a minimal basis set for C ($r_c = 4.4, 4.7$), N ($r_c = 4.4, 4.7$), O ($r_c = 3.6, 4.1$), S ($r_c = 4.5, 5.0$), and Ti ($r_c = 6.3, 6.3, 5.7$), adding a 4p^0-state to Ti ground-state configuration for polarization; the r_c values in the parentheses are the cutoff of the wavefunctions (in atomic units) for s, p and d shells, respectively.

To quantify the effects of doping concentration on the photoresponse in the anion-doped TiO$_2$ systems, we calculate the degree of localization for electronic states near the band edge. We introduce a parameter, W, which gives the number of accessible atoms in a particular electronic state and describes the spatial extent of this state [39]. For a particular state ν, the wavefunction $\Phi(\nu)$ has a Mulliken population $p_i(\nu)$ on atom i, which loosely is considered the probability that an electron is in state ν and resides on particular atom i. The populations are normalized, $\sum_i p_i(\nu) = 1$. From probability theory, we define a quantum entropy for state ν as $S(\nu) = -\sum_i p_i(\nu) \ln p_i(\nu)$. From Boltzmann's equation, we can determine the
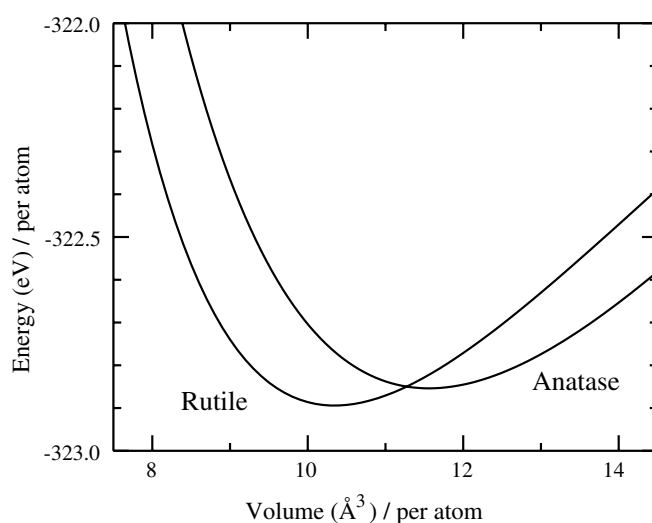
Figure 1. Theoretical equation of state for the TiO_2 in rutile and anatase structures.

number of accessible atoms $W(\nu)$ for a given electronic state $W(\nu) = e^{S(\nu)}$. The number of accessible atoms $W(\nu)$ gives a quantitative, and easily calculable, measure of how many atoms a particular electronic state $\Phi(\nu)$ reaches.

3. Electronic and structural properties of bulk TiO_2

In predicting the electronic structures of the anion-doped TiO_2 systems, we first examine the electronic structure of the bulk TiO_2 in the rutile and anatase structures for comparison. Rutile and anatase TiO_2 are both tetragonal. The tetragonal rutile structure belongs to the space group $P4_2/mnm$ (D_{4h}^{14}) [40], containing 6 atoms per primitive unit cell. Tetragonal anatase structure belongs to the space group $I4_1/amd$ (D_{4h}^{19}) [40], containing 12 atoms per conventional unit cell. Structural parameters for both rutile and anatase have been determined to a high degree of accuracy from the neutron diffraction experiments performed by Burdett *et al* [41]. We obtain optimal structures by minimizing the total energy of the rutile and anatase TiO_2 with respect to the lattice parameters a, c, and internal parameter u. We then find the ground-state structure by fitting the theoretical values of energy and volume to an integrated equation of state (EOS) using the third-order Birch–Murhaghan [42] form, which are based on the elastic properties of the solid.

The structural properties of bulk TiO_2 are summarized in table 1. We correctly predict that rutile has a smaller volume and lower energy at its equilibrium structure compared to that of anatase (see figure 1); the rutile structure is the more stable phase of TiO_2, which is consistent with theory and experiment [43]. From the integrated EOS, we obtain the bulk modulus B of 206 and 183 GPa in rutile and anatase, respectively. These values agree well with the experimental values of 211 GPa [44] in rutile and 179 GPa [44] in anatase. Our results are also consistent with the calculated results of others [45–48]. Our results for the structural parameters in both rutile and anatase structures are in excellent agreement, being within 1% of the experimental results of Burdett *et al* [41].

From our theoretically predicted equilibrium structure, we calculate the self-consistent electronic band structures for the rutile (left panel in figure 2) and anatase (right panel in figure 2) structures along the high-symmetry directions of irreducible Brillouin zone. For the

Table 1. Theoretically determined structural and elastic parameters for TiO_2 in the rutile and anatase structures. The experimental values are in parentheses. The results from other theoretical calculations are also listed.

	Rutile	Anatase
Volume ($\text{Å}^3/TiO_2$)		
Present work	30.88 (31.21 [41])	34.54 (34.07 [41])
Other calc.	32.42 [45], 31.88 [46]	34.27 [47]
Lattice const. a (Å)		
Present work	4.575 (4.593 [41])	3.797 (3.785 [41])
Other calc.	4.653 [45], 4.589 [46]	3.692 [47]
Lattice const. c (Å)		
Present work	2.951 (2.959 [41])	9.575 (9.512 [41])
Other calc.	2.965 [45], 2.965 [46]	9.471 [47]
Internal parameter u		
Present work	0.303 (0.303 [41])	0.208 (0.208 [41])
Other calc.	0.305 [45], 0.304 [46]	0.206 [47]
Bulk modulus (GPa)		
Present work	206 (211 [44])	183 (179 [44])
Other calc.	240 [45], 209 [46]	272 [46], 194 [48]

rutile structure (left panel in figure 2), the calculated direct band gap from Γ to Γ of 3.05 eV is in agreement with the reported experimental gap of 3.06 eV [49]. The LDA generally underestimates the experimental band gap for insulators and semiconductors, and the band gap obtained from *ab initio* plane-wave calculations for TiO_2 is around 2.0 eV [45]. This underestimating effect of the LDA is compensated in our results because we use a local orbital basis set. We also find an indirect band gap from Γ to M which is smaller than the direct band gap by 0.13 eV. This finding is in agreement with the theoretical prediction based on tight-binding (TB) [50] and linear muffin-tin orbital (LMTO) [51] calculations. We find both direct and indirect band gaps as well in the anatase structure. For anatase, the direct band gap from Γ to Γ of 3.26 eV is in agreement with the experimentally observed gaps of 3.20 [52] and 3.42 eV [53]. Unlike rutile, the top of the valence band is at M and the bottom of conduction band is at Γ in the anatase structure. This indirect band gap of 3.0 eV is smaller than that of the direct gap by about 0.26 eV, which is consistent with the results obtained by Mo and Ching [46].

Similar features of the electronic band structures for the rutile and anatase structures are observed as shown in figure 2. We have calculated the electronic density of states (DOS) for both structures, which are depicted in figure 3, to represent the detailed feature of the electronic structure in the systems as a comparison for the anion-doped structures. Table 2 gives a summary of our electronic structure results in comparison to experiments and calculations of others for the detailed features of the band structures. The DOS shows that the lower energy bands around −17 eV result from a predominantly oxygen 2s (O_{2s}) character with a width of 1.89 eV for the rutile structure and 1.80 eV for the anatase structure, respectively. The upper valence bands are composed mainly of O_{2p} orbitals and have a width of 5.75 eV (4.86 eV) in the rutile (anatase) structure. These results are in agreement with the experimental ranges of 5.50 eV [54] (4.75 eV [52]). On the other hand, the lower conduction bands, composed primarily of unoccupied Ti_{3d} states, have a full width of 5.8 eV for the rutile structure and 5.6 eV for the anatase structure, respectively. These results are consistent with other theoretical predictions [45–47].
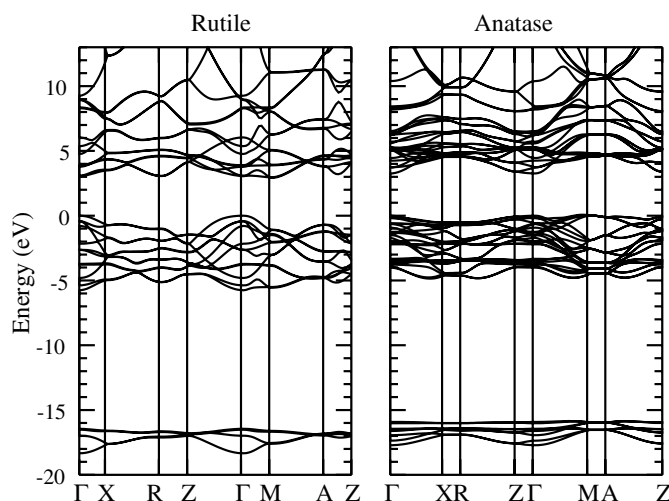
Figure 2. Band structures for bulk TiO_2 in the rutile (left panel) and anatase (right panel) structures. The valence band maximum is taken as the zero of energy.
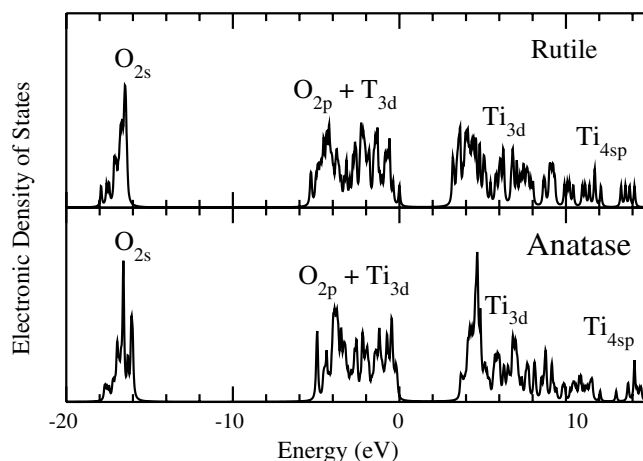

Figure 3. Electronic density of states (DOS) for bulk TiO_2 in the rutile (upper panel) and anatase (lower panel) structures, respectively. The valence band maximum is taken as the zero of energy.

4. Carbon-doped TiO_2

The results of bulk TiO_2 provide an excellent basis to explore the electronic properties of the anion (C, N, and S)-doped TiO_2 systems. Using the theoretically determined lattice parameters from our equilibrium structure, we construct supercells of TiO_2 for both the rutile and anatase structures containing 64 primitive unit cells (384 atoms in total). We build the anion-doped structures from this initial TiO_2 supercell. Two concentrations of carbon doping are considered: (1) one oxygen atom is randomly substituted by carbon, yielding a doping concentration of 0.26%; (2) 20 oxygen sites are randomly substituted by carbon, yielding a 5.20% doping concentration. The DOSs for the undoped TiO_2 supercells (bulk) and carbon-doped TiO_2 (called $TiO_{2-x}C_x$), as well as the species-projected DOS are depicted in figure 4. The species-
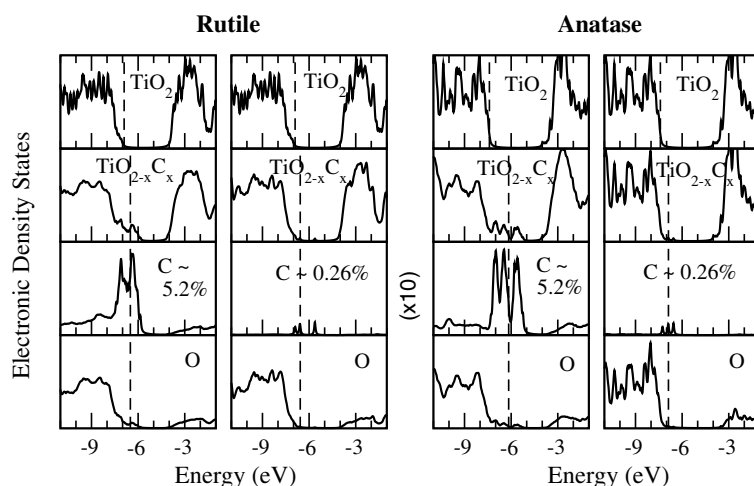
Figure 4. The DOSs for carbon-doped rutile and anatase TiO$_2$. The DOSs for both rutile and anatase structures at two different carbon doping concentrations of 5.2% (left) and 0.26% (right) are presented, respectively. The dashed line indicates the valence band edge in the system. The top panel shows the DOS for bulk TiO$_2$ as a reference, the second panel shows the carbon-doped (TiO$_{2-x}$C$_x$) structure, and the third and lowest panels show the species-projected DOSs onto carbon and oxygen atoms, respectively. The scale for the species-projected DOS onto carbon is ten times larger than the other DOS plots.

Table 2. Comparison of our present work to the experimentally determined electronic properties for TiO$_2$ in the rutile and anatase structures. Here E_g is direct bandgap (from Γ to Γ), while E_{VB} is the upper valence bandwidth.

	Rutile	Anatase
	E_g (eV)	
Present work	3.05	3.26
Experiments	3.06 [49]	3.20 [52], 3.42 [53]
Other calc.	2.00 [45], 1.78 [46]	2.22 [46], 2.00 [47]
	E_{VB} (eV)	
Present work	5.75	4.86
Experiments	5.50 [54]	4.75 [52]
Other calc.	5.70 [45], 6.22 [46]	5.17 [46], 5.05 [47]

projected DOS is determined by the contribution to the DOS from a chosen set of atoms, such as C or O. The species-projected DOSs onto carbon and oxygen atoms are depicted in the lower panels of figure 4. The scale for the species-projected DOS onto carbon is ten times larger than the other DOS plots. The dashed lines in the DOS figures indicate the valence band edge of the systems. The results for carbon-doped rutile TiO$_2$ which have been discussed in our previous work [19] are also included for comparison. In the following, we mainly focus our discussion on the electronic properties of carbon-doped anatase TiO$_2$.

Comparison of the bulk TiO$_2$ DOS with the DOSs of corresponding carbon-doped structures indicates that the conduction band minimum remains unchanged by carbon doping. This affirms that carbon-doped TiO$_2$ satisfies the requirement as an efficient photocatalytic material since its conduction band remains above the redox potentials of many substrates [3].

The DOS comparison also indicates that new states above the valence band edge of the bulk TiO$_2$ are introduced in carbon-doped structures. Analysis of the species-projected DOSs onto carbon atoms (third panels in figure 4 for both rutile and anatase) show that these states, as well as the states penetrating into the upper valence band of the bulk TiO$_2$ (which is composed of O$_{2p}$ states), are carbon 2p states introduced by doping, and only about half of these states are filled states. As a result of the substitutional carbon atoms being incorporated, the valence band edge shifts to high energy compared with the bulk TiO$_2$ and the bandgap narrows. Similar phenomena have been observed experimentally and theoretically, as several studies have reported a red shift in the absorption spectra [15–18, 20]. Irie *et al* [17] and Khan *et al* [16] both show energy levels just above the valence energy of the bulk samples which corresponds to *substitutional* carbon dopants. They also conclude that the substitutional carbon atoms are responsible for the visible light absorption.

In the structures of 5.2% carbon concentration (see figure 4 for both rutile and anatase structures), the new valence band states introduced by carbon are quite continuous and there is a significant energy red shift in the valence band edge. As a consequence, the corresponding band gap is narrowed down to 2.0 eV for the anatase structure (2.35 eV for rutile). Experiments by Khan *et al* [16] show two optical absorption thresholds, in the visible-light region, at 535 nm (bandgap of 2.32 eV) and 440 nm (bandgap of 2.82 eV) in samples of estimated carbon concentration around 5%. They conclude that these two absorption thresholds probably result from the two different compositions of the carbon-doped TiO$_2$, i.e., anatase and rutile structures, respectively. Meanwhile, a much higher efficiency in water dissociation was obtained in their experiments which significantly improves the original Fujishima and Honda experiments [1]. Contrarily, a much lower efficiency was observed by Irie *et al* [17] in carbon-doped TiO$_2$ samples of estimated carbon concentration around 0.32%. They conclude that the much lower quantum efficiency than that expected to be observed probably results from the lower doping concentration in the samples, although a small shift of absorption edge to the visible-light region is detected. Our lower concentration results show that carbon states are isolated and slightly alter the TiO$_2$ valence states. This leads itself to a probable explanation of the low concentration experimental results.

As a quantitative measure of localization, we plot, in figure 5, the number of accessible atoms, $W(\nu)$, for each electronic state near the valence band edge in the carbon-doped TiO$_2$; for each carbon-doped TiO$_2$ structure, rutile or anatase, 5.20% carbon concentration is represented by the top panel while the bottom panel represents 0.26% carbon concentration. The dashed line indicates the valence band edge in the electronic structures. At lower carbon concentration the top valence band state is very localized and the wavefunction does not overlap significantly with oxygen atoms. As a result, the mobility of a hole created there will be quite poor and this explains why the photocatalytic efficiency could be small at low concentration. The results for higher carbon concentration follow the opposite trend: the states near the valence band edge are less localized, and there is significant overlap with the oxygen atoms. Furthermore, comparison of the results between different concentrations indicates that the higher concentration case has more occupied states near the valence band edge. This may explain why a higher concentration of carbon would produce visible absorption with larger photocatalytic efficiency overall.

An interpretation given by Asahi *et al* [20], which we support, is that the states in the gap should overlap sufficiently with the O 2p states to transfer photoexcited carriers to reactive sites at the catalyst surface within their lifetime. Our DOS calculations, the left panels of species-projected DOSs into carbon and oxygen atoms in both rutile and anatase structures, show that there is significant overlap between the carbon states and O$_{2p}$ states for 5.20% carbon concentration structures. On the other hand, in the lower carbon concentration structures (the right panels of species-projected DOSs into carbon and oxygen atoms in both rutile and anatase
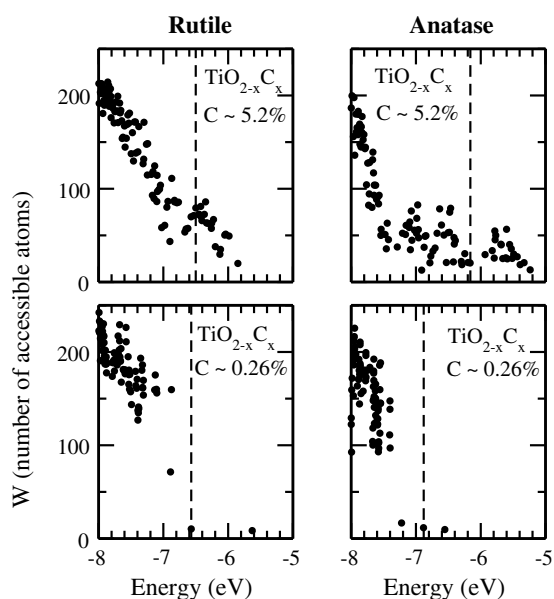
Figure 5. Number of accessible atoms, W, for each electronic state near the valence band edge in the carbon-doped rutile and anatase TiO_2. The W for both rutile and anatase structures at two different carbon doping concentrations of 5.2% (top) and 0.26% (bottom) are presented, respectively. The dashed line indicates the valence band edge in the system.

structures), the states introduced by carbon dopants are quite distinct and highly localized on the single carbon dopant state. There is no significant overlap observed for the structures of 0.26% carbon concentration. Furthermore, the energy shift of the valence band edge is much smaller compared with the high doping concentration structures. Consequently, we predict that the photocatalytic performance for lower carbon concentrations should be much lower than that of higher carbon concentrations in the carbon-doped rutile and anatase TiO_2.

5. Nitrogen-doped TiO_2

Extensive studies have recently proposed that nitrogen-doped TiO_2 is also a promising second-generation photocatalytic material [20–25]. Experimental results for doping with nitrogen indicate there is a significant red shift in the absorption spectra [20], which yields photoactivity in the visible. There is some debate as to whether nitrogen dopant in TiO_2 is interstitial or substitutional [20, 23]. The experiments by Diwald *et al* [23] show that the interstitial nitrogen dopant is effective in reducing the threshold photon energy for photochemistry from 3.0 to 2.4 eV, which is a shift of 0.6 eV into the visible region. Their result disagrees with the conclusion of Asahi *et al* [20], who reported that nitride ions that substitute for O^{2-} ions in the TiO_2 lattice are the necessary dopant species for TiO_2 photocatalysis in the visible region. As a comparison with our carbon-doped results, we examine substitutional nitrogen doping.

Due to nitrogen's odd number of valence electrons, we replace two oxygen atoms by nitrogen, resulting in a 0.52% concentration for the lower concentration scenario. The DOSs for the bulk and nitrogen-doped TiO_2 (called $TiO_{2-x}N_x$) are presented in figure 6; the species-projected DOSs onto nitrogen and onto oxygen are depicted in the lower panels. The scale for the species-projected DOS onto nitrogen is ten times larger than the other DOS plots. The
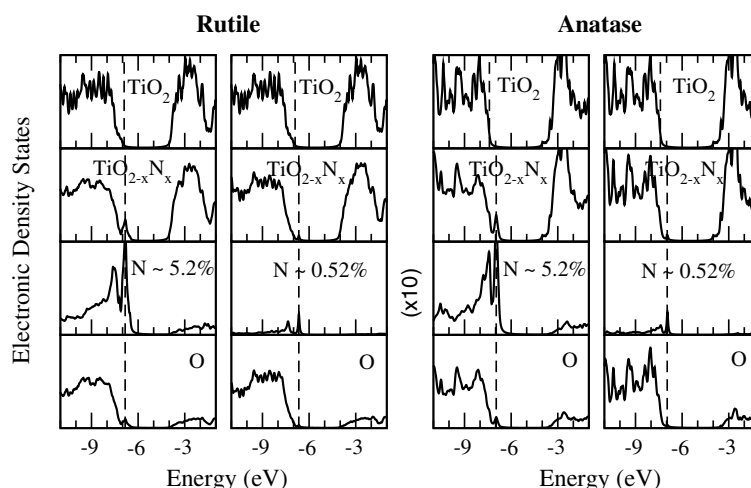
Figure 6. The DOSs for the nitrogen-doped rutile and anatase TiO$_2$. The DOSs for both rutile and anatase structures at two different nitrogen doping concentrations of 5.2% (left) and 0.26% (right) are presented, respectively. The dashed line indicates the valence band edge in the system. The top panel shows the DOS for bulk TiO$_2$ as a reference, the second panel shows the nitrogen-doped (TiO$_{2-x}$N$_x$) structure, and the third and lowest panels show the species-projected DOSs onto nitrogen and oxygen atoms, respectively. The scale for the species-projected DOS onto nitrogen is ten times larger than the other DOS plots.

dashed lines in the DOS figures indicate the valence band edge of the systems. The conduction band minimum remains unchanged which indicates that the nitrogen-doped TiO$_2$ satisfies the requirement for obtaining a versatile photocatalytic material. The new states just above the valence band edge of the bulk TiO$_2$ and the states penetrating into the upper valence band of the bulk TiO$_2$ are nitrogen 2p states introduced by doping; only parts of these states are occupied. The number of accessible atoms, W, a quantitative measure of localization of the electronic states in the nitrogen-doped TiO$_2$, is depicted in figure 7.

In carbon-doped rutile TiO$_2$ we have obtained that both high and low doping concentrations shifted the valence band edge up by 0.7 eV [19]. However, in nitrogen-doped rutile TiO$_2$, there is no significant energy shift (<0.05 eV) in the valence band edge for higher nitrogen concentration (5.2%) with our calculated structure. A significant shift is observed only in the lower nitrogen doping concentration (0.52%), which results in a narrowed band gap of 2.55 eV. From our DOS calculations (see figure 6) we conclude that lower doping concentrations produce a greater improvement in photoactivity in the visible. The red shift of the valence band edge found in this work is in agreement with experimental observations [20]. Combined with their theoretical analysis and experimental observations, Asahi *et al* [20] state that the active sites of nitrogen for photocatalysis under visible light are the substitutional ones with an estimated doping concentration of 0.38%.

There is no significant overlap between the nitrogen states and O$_{2p}$ states for 0.52% nitrogen concentration structures. Furthermore, the results of number of accessible atoms (see figure 7 for the rutile structure) also indicate that at lower nitrogen concentration the valence band edge is more localized compared with higher concentration nitrogen-doped rutile TiO$_2$. Comparing the results of carbon-doped with nitrogen-doped rutile TiO$_2$, we can conclude that the incorporation of carbon dopants produces a narrower band gap than that of nitrogen, regardless of doping concentration for the rutile TiO$_2$. As a result, the carbon-doped TiO$_2$
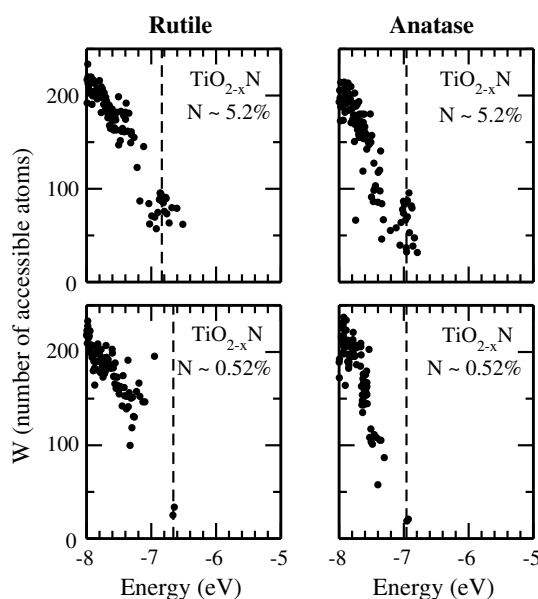
Figure 7. Number of accessible atoms, W, for each electronic state near the valence band edge in the nitrogen-doped rutile and anatase TiO$_2$. The W for both rutile and anatase structures at two different nitrogen doping concentrations of 5.2% (top) and 0.26% (bottom) are presented, respectively. The dashed line indicates the valence band edge in the system.

materials are able to absorb energy in the visible light region more efficiently than the nitrogen-doped materials, and they provide higher photocatalytic efficiency due to the less localized states at higher concentrations.

Unlike nitrogen-doped rutile TiO$_2$, the same amounts of shifts of about 0.44 eV are obtained in nitrogen-doped anatase TiO$_2$ for both higher and lower doping concentrations, resulting in a band gap of 2.82 eV (440 nm). The red shift of the valence band edge found in this work agrees well with experiments and theories [20, 22, 24, 25]. Our DOS calculations show that there is significant overlap between the nitrogen states and O$_{2p}$ states for 5.20% carbon concentration structures. On the other hand, in the lower carbon concentration structures, the states introduced by nitrogen dopants are quite distinct and highly localized on the single dopant state. There is no significant overlap observed for the structures of 0.52% nitrogen concentration. As an analogy to the discussion of the carbon-doped case, we can conclude that the higher concentration in nitrogen-doped anatase TiO$_2$ will be likely to produce higher photocatalytic performance in the visible light region.

Similiar to the carbon-doped case, for the higher doping concentration case, the more occupied states near the valence band edge may have the chance to participate in the photo reaction under visible light. Therefore, a higher concentration of nitrogen would produce both visible absorption with larger photocatalytic efficiency overall in the nitrogen-doped anatase TiO$_2$. Comparing the results of carbon-doped with nitrogen-doped anatase TiO$_2$, we can see that the incorporation of carbon dopants produces a narrower band gap than that with incorporation of nitrogen. As a result, the carbon-doped TiO$_2$ materials are able to absorb energy in the visible light region more efficiently than the nitrogen-doped materials, and they provide higher photocatalytic efficiency.
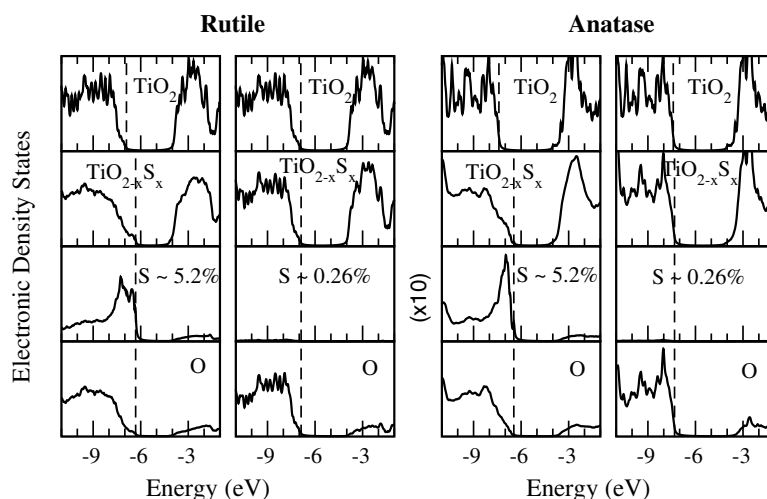
Rutile **Anatase**

Figure 8. The DOSs for the sulfur-doped rutile and anatase TiO_2. The DOSs for both rutile and anatase structures at two different sulfur doping concentrations of 5.2% (left) and 0.26% (right) are presented, respectively. The dashed line indicates the valence band edge in the system. The top panel shows the DOS for bulk TiO_2 as a reference, the second panel shows the sulfur-doped ($TiO_{2-x}N_x$) structure, and the third and lowest panels show the species-projected DOSs onto sulfur and oxygen atoms, respectively. The scale for the species-projected DOS onto sulfur is ten times larger than the other DOS plots.

6. Sulfur-doped TiO_2

Although a previous theoretical study showed that sulfur doping in TiO_2 contributes to band gap narrowing, sulfur doping is difficult to achieve due to large formation energies required for substituting S for O in TiO_2 [20]. Contrary to this expectation, sulfur-doped anatase TiO_2 polycrystalline powder, including S substituted for O, was synthesized by oxidative heating of titanium disulfide (TiS_2) powder. Sulfur doping causes a photon-to-carrier conversion in the energy region below the band gap of pure TiO_2 [26, 27]. The photocatalyst applications of sulfur-doped TiO_2, therefore, are of great importance. In this section, we present results for sulfur-doped rutile and anatase TiO_2. The supercells of sulfur-doped TiO_2 are constructed in the same way as was done for the carbon-doped TiO_2 structures.

The DOSs of the bulk and sulfur-doped rutile and anatase TiO_2 (called $TiO_{2-x}S_x$) are presented, respectively, in the upper panels of figure 8; the species-projected DOSs onto sulfur and oxygen atoms are also depicted in the lower panels. The scale for the species-projected DOS onto sulfur is ten times larger than the other DOS plots. The dashed lines in the DOS figures indicate the valence band edge of the systems. In the lower doping concentration (0.26%) of sulfur-doped TiO_2 (right panels in figure 8 for each structure), there is no significant shift of the valence band edge observed. This implies that lower doping concentration yields very poor performance as a photocatalytic material due to the large band gap in such systems (>3 eV). In contrast, a significant red shift of the valence band edge is obtained at higher doping concentration in both rutile and anatase structures, and the corresponding band gaps are narrowed down to 2.3 and 2.2 eV, respectively. Our results concerning the band gap narrowing and the concentration dependence of photoactivity in the sulfur-doped TiO_2 are in agreement with the experimental observations and theoretical conclusions in the literature [26–29].
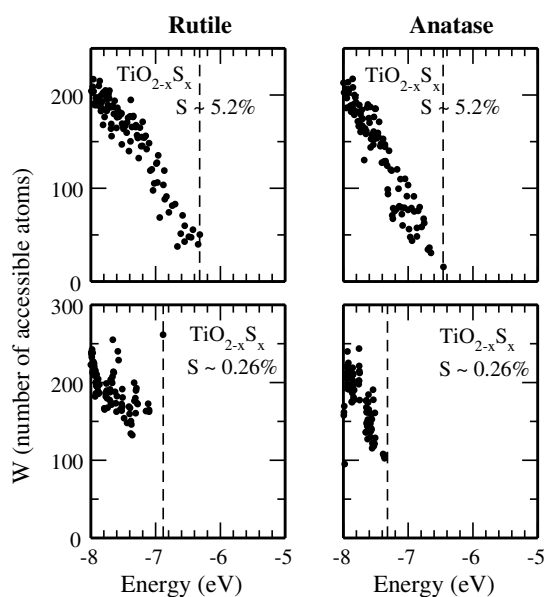
Figure 9. Number of accessible atoms, W, for each electronic state near the valence band edge in the sulfur-doped rutile and anatase TiO_2. The W for both rutile and anatase structures at two different sulfur doping concentrations of 5.2% (top) and 0.26% (bottom) are presented, respectively. The dashed line indicates the valence band edge in the system.

The number of accessible atoms, $W(\nu)$, for sulfur-doped rutile and anatase TiO_2 with concentrations of 5.20% (top) and 0.26% (bottom) are illustrated in figure 9, respectively. The dashed line indicates the valence band edge of these systems. In figure 9 a different y-axis scale is used in the lower concentration case to show the very delocalized valence band edge state. The scale for the higher doping concentration remains the same as for the carbon- and nitrogen-doped cases. In contrast to the carbon- and nitrogen-doped TiO_2, the valence band edge is very delocalized for the lower concentration in the sulfur-doped TiO_2. However, since the valence band edge remains virtually unchanged in this case, there is no high photoactivity expected to be detected in the visible light region. For the higher sulfur doping concentration, photocatalytic activity in the visible light region should be observed and it should be more efficient than in the lower concentration case due to both the band gap narrowing effect and the delocalization of the valence band edge. By comparing figure 9 with figures 5 and 7, we conclude that sulfur-doped TiO_2 produces the smallest photoresponse in the visible light region among the anion dopants discussed in this work.

7. Discussion and conclusion

In conclusion, the electronic properties of the bulk and anion (C, N, and S)-doped TiO_2 materials are precisely determined using FIREBALL, an *ab initio* electronic-structure method. Our theoretical predictions concerning the photoresponse in the promising second-generation photocatalytic materials, anion-doped TiO_2, are consistent with the available experimental results. From the available experimental evidences and our theoretical results, we conclude that both bandgap narrowing and the overlap between the O 2p state and dopant-introduced states strongly affect the photoactivities of doped TiO_2 materials. Among those anion dopants

discussed, we propose that carbon is the most promising candidate for second-generation photocatalytic materials based on TiO_2.

Acknowledgments

References

[1] Fujishima A and Honda K 1972 *Nature* **238** 37
[2] Frank N S and Bard A J 1977 *J. Phys. Chem.* **81** 1481
[3] Hagfeldt A and Graetzel M 1995 *Chem. Rev.* **95** 49
[4] Einaga H, Futamura S and Ibusuki T 1999 *Phys. Chem. Chem. Phys.* **1** 4903
[5] Halmann M M and Steinberg M 1999 *Greenhouse Gas Carbon Dioxide Mitigation: Science and Technology* (Boca Raton, FL: CRC Press)
[6] Hashimoto K, Ishibashi K and Watanabe T 2002 *Photocatalysis: Science and Technology* (Tokyo: Kodansha, Springer)
[7] Fujishima A, Rao T N and Tryk D A 2000 *J. Photochem. Photobiol.* C **1** 1
[8] Hoffmann M R, Martin S T and Choi W 1995 *Chem. Rev.* **95** 69
[9] Kaneko M and Ohkura 2002 *Photocatalysis* (Tokyo: Springer)
[10] Ollis D F and Al-Ekabi H 1993 *Photocatalysis Purification and Treatment of Water and Air* (New York: Elsevier Science)
[11] Choi W, Termin A and Hoffman M R 1994 *J. Phys. Chem.* **98** 13669
[12] Karakitsou H and Verykios X E 1993 *J. Phys. Chem.* **97** 1184
[13] Yamashita H, Ichihashi Y, Takeuchi M, Kishiguchi S and Anpo M 1999 *J. Synchrotron Radiat.* **6** 451
[14] Anpo M 2000 *Green Chemistry* (Oxford: Oxford University Press)
[15] Sakthivel S and Kisch H 2003 *Angew. Chem. Int. Edn* **42** 4908
[16] Khan S U M, Al-Shahry M and Ingler W B 2002 *Science* **297** 2243
[17] Irie H, Watanabe Y and Hashimoto K 2003 *Chem. Lett.* **32** 772
[18] Noworyta K and Augustynski J 2004 *Electrochem. Solid.-State. Lett.* **7** E31
[19] Wang H and Lewis J P 2005 *J. Phys.: Condens. Matter* **17** L209
[20] Asahi R, Morikawa T, Ohwaki T, Aoki K and Taga Y 2001 *Science* **293** 269
[21] Lindgren T, Mwabora J M, Avendaño E, Jonsson J, Granqvist C G and Lindquist S E 2003 *J. Phys. Chem.* A **107** 5709
[22] Irie H, Watanabe Y and Hashimoto K 2003 *J. Phys. Chem.* B **107** 5483
[23] Diwald O, Thompson T L, Zubkov T, Goralski E G, Walck S D and Yates J T 2004 *J. Phys. Chem.* B **108** 6004
[24] Yang S W and Gao L 2004 *J Am. Ceram. Soc.* **87** 1803
[25] Di Valentin C, Pacchioni G and Selloni A 2004 *Phys. Rev.* B **70** 085116
[26] Umebayashi T, Yamaki T, Tanaka S and Asai K 2003 *Chem. Lett.* **32** 330
[27] Umebayashi T, Yamaki T, Itoh H and Asai K 2002 *Appl. Phys. Lett.* **81** 454
[28] Yamamoto T, Yamashita Y, Tanaka I, Matsubara F and Muramatsu A 2004 *Mater. Trans.* **45** 1987
[29] Umebayashi T, Yamaki T, Yamamoto S, Miyashita A, Tanaka S, Sumita T and Asai K 2003 *J. Appl. Phys.* **93** 5156
[30] Lewis J P, Glaesemann K R, Voth G A, Fritsch J, Demkov A A, Ortega J and Sankey O F 2001 *Phys. Rev.* B **64** 195103
[31] Adams G B, O'Keefe M, Demkov A A, Sankey O F and Huang Y M 1994 *Phys. Rev.* B **49** 8048
[32] Demkov A A, Ortega J, Sankey O F and Grumbach M P 1995 *Phys. Rev.* B **52** 1618
[33] Sankey O F, Demkov A A, Windl W, Fritsch J, Lewis J P and Fuentes-Cabrera M 1998 *Int. J. Quantum Chem.* **69** 327
[34] Wang H, Lewis J P and Sankey O F 2004 *Phys. Rev. Lett.* **93** 016401
[35] Harris J 1985 *Phys. Rev.* B **31** 1770
[36] Foulkes W and Haydock R 1989 *Phys. Rev.* B **39** 12520
[37] Sankey O F and Niklewski D J 1989 *Phys. Rev.* B **40** 3979
[38] Finnis M W 1990 *J. Phys.: Condens. Matter* **2** 331
[39] Lewis J P, Cheatham T E, Starikov E B, Wang H and Sankey O F 2003 *J. Phys. Chem.* B **107** 2581
[40] Hahn T 1983 *International Table of Crystallography* Vol A *Space-Group Symmetry* (Dordrecht: Reidel)

[41] Burdett J K, Hughbanks T, Miller G J, Richardson J W and Smith J V 1987 *I. Am. Chem. Soc.* **109** 3639
[42] Birch F 1947 *Phys. Rev.* **71** 809
[43] Muscat J, Swamy V and Harrison N M 2002 *Phys. Rev.* B **65** 224112 and references therein
[44] Arlt T, Bermejo M, Blanco M A, Gerward L, Jiang J Z, Olsen J S and Recio J M 2000 *Phys. Rev.* B **61** 14414
[45] Glassford K M and Chelikowshy J R 1992 *Phys. Rev.* B **46** 1284
[46] Mo S D and Ching W Y 1995 *Phys. Rev.* B **51** 13023
[47] Asahi R, Taga Y, Mannstadt W and Freeman A J 2000 *Phys. Rev.* B **61** 7459
[48] Dewhurst J K and Lowther J E 1996 *Phys. Rev.* B **54** R3673
[49] Pascual J and Mathieu H 1978 *Phys. Rev.* B **18** 5606
[50] Vos K 1977 *J. Phys. C: Solid State Phys.* **10** 3917
[51] Kasowski R V and Tait R H 1979 *Phys. Rev.* B **20** 5168
[52] Sanjinès R, Tang H, Berger H, Gozzo F, Margaritondo G and Lèvy F 1994 *J. Appl. Phys.* **75** 2945
[53] Tang H, Lèvy F, Berger H and Schmid P E 1995 *Phys. Rev.* B **52** 7771
[54] Kowalczyk S P, McFeely F R, Ley L, Gritsyna V T and Shirley D A 1977 *Solid State Commun.* **23** 161